



**POLITECNICO**  
MILANO 1863

[RE.PUBLIC@POLIMI](mailto:RE.PUBLIC@POLIMI)

Research Publications at Politecnico di Milano

## Post-Print

This is the accepted version of:

D. Gusmini, A. D'Ambrosio, S. Servadio, P.M. Siew, P. Di Lizia, R. Linares  
*Effects of Orbit Raising and Deorbiting in Source-Sink Evolutionary Models*  
Journal of Spacecraft and Rockets, published online 07/01/2024  
doi:10.2514/1.A35849

The final publication is available at <https://doi.org/10.2514/1.A35849>

Access to the published version may require subscription.

**When citing this work, cite the original published paper.**

Permanent link to this version

<http://hdl.handle.net/11311/1259264>

# Effects of Orbit Raising and Deorbiting in Source-Sink Evolutionary Models\*

Davide Gusmini<sup>†</sup>, Andrea D'Ambrosio<sup>‡</sup>, Simone Servadio<sup>§</sup>, Peng M. Siew<sup>¶</sup>  
*Massachusetts Institute of Technology, Cambridge, Massachusetts 02139.*

Pierluigi Di Lizia<sup>||</sup>  
*Polytechnic University of Milan, 20156 Milan, Italy.*

Richard Linares<sup>\*\*</sup>  
*Massachusetts Institute of Technology, Cambridge, MA 02139, USA.*

The sustainability of the Low Earth Orbit (LEO) environment is threatened by the growing number of Anthropogenic Space Objects planned to be launched in the coming years. This paper investigates the evolution of objects residing in LEO through the MIT Orbital Capacity Assessment Tool (MOCAT), an evolutionary multi-shell multi-species source-sink model. The proposed novelty considers the flow of objects crossing multiple shells during orbit raising and deorbiting maneuvers, modeled through the secular variation of the semi-major axis under a low-thrust continuous applied control. To this aim, a higher fidelity MOCAT version including active satellites, derelicts, debris, and rocket bodies has been developed and used. The results demonstrate that incorporating orbit transfer fluxes into the model results in a higher number of collisions, which leads to a greater quantity of debris and poses a greater threat to the safety of low Earth orbit.

## Nomenclature

$a$	=	Semi-major axis [km]
$A$	=	Area of an object [ $\text{m}^2$ ]
$B_c$	=	Ballistic coefficient [ $\text{m}^2/\text{kg}$ ]

---

\*Paper presented at the 33rd AAS/AIAA Space Flight Mechanics Meeting (15-19 January 2023, Austin, TX, USA). Paper number: 23-156.

<sup>†</sup> *Corresponding Author.* Graduate student, Department of Aeronautics and Astronautics, 77 Massachusetts Avenue, Massachusetts Institute of Technology, MA 02139, USA. email: gusmini.dav@gmail.com

<sup>‡</sup> Postdoctoral Associate, Department of Aeronautics and Astronautics, 77 Massachusetts Avenue, Massachusetts Institute of Technology, MA 02139, USA. email: andreadam93@gmail.com

<sup>§</sup> Postdoctoral Associate, Department of Aeronautics and Astronautics, 77 Massachusetts Avenue, Massachusetts Institute of Technology, MA 02139, USA. email: servadio@iastate.edu

<sup>¶</sup> Postdoctoral Associate, Department of Aeronautics and Astronautics, 77 Massachusetts Avenue, Massachusetts Institute of Technology, MA 02139, USA. email: siewpm@mit.edu

<sup>||</sup> Associate Professor, Department of Aerospace Science and Technology, 20156 Milano, Italy. email: pierluigi.dilizia@polimi.it

<sup>\*\*</sup> Rockwell International Career Development Professor, Associate Professor of Aeronautics and Astronautics, Department of Aeronautics and Astronautics, 77 Massachusetts Avenue, Massachusetts Institute of Technology, MA 02139, USA. email: linaresr@mit.edu

$c_D$	=	Drag coefficient
$\dot{C}$	=	Number of objects removed/added per year due to a collision
$\dot{C}_{add}$	=	Gain in derelicts and debris per year due to a collision
$\dot{C}_{PMD}$	=	Number of objects removed per year due to Post-Mission Disposal
$d$	=	Thickness of the shell [km]
$D$	=	Derelicts
$\dot{F}$	=	Flux due to the atmospheric drag and orbit transfer maneuvers [objects/year]
$h$	=	Altitude of the Shell [km]
$L_C$	=	Characteristic Length [m]
$M$	=	Mass of the objects involved in a catastrophic collision [kg]
$M_p$	=	Mass of the projectile in a non-catastrophic collision [kg]
$m$	=	Mass of a generic object [kg]
$n_f$	=	Number of fragment generated from a collision
$N$	=	Trackable Debris
$N_s$	=	Number of species considered
$P_d$	=	Probability of success of raising maneuver
$P_m$	=	Probability of success of post-mission disposal
$P_r$	=	Probability of success of deorbiting maneuver
$Q$	=	Generic species
$R$	=	Distance from the center of the Earth [km]
$r$	=	Radius of the object [m]
$S$	=	Active satellites
$t_{depl}$	=	Deployment time [year]
$\mathbf{T}$	=	Diagonal matrix dependent on the time required to cross each shell
$v$	=	Change in semi-major axis [km/s]
$v_{imp}$	=	Impact velocity in a non-catastrophic collision [km/s]
$V(h)$	=	Volume of the orbital shell [km <sup>3</sup> ]
$\alpha$	=	Fractions of collisions that an active satellite fails to avoid (only with derelicts and tracked debris)
$\alpha_a$	=	Fractions of collisions that an active satellite fails to avoid (only among active satellites)
$\Delta t$	=	Satellite operation life [years]
$\delta$	=	Ratio of the density of disabling to lethal trackable debris involving satellites and derelicts
$\delta_B$	=	Ratio of the density of disabling to lethal trackable debris involving rocket bodies

- $\epsilon$  = Magnitude of the low thrust acceleration
- $\Theta_h^{+,-}$  = Diagonal matrices representing the transition to and from the operating satellite category
- $\Theta_r^{+,-}$  = Diagonal matrices describing the flow of satellites due to raising maneuvers
- $\Theta_d^{+,-}$  = Diagonal matrices describing the flow of satellites due to deorbit maneuvers
- $\Gamma$  = Matrix of coefficients
- $\lambda$  = Annual Launch Rate [objects/year]
- $\mu$  = Earth gravitational parameter [ $\text{km}^3/\text{s}^2$ ]
- $\phi_{ij}$  = Intrinsic probability of collision matrix [1/year]
- $\rho$  = Atmospheric density [ $\text{kg}/\text{m}^3$ ]
- $\sigma_{ij}$  = Impact Parameter [ $\text{m}^2$ ]
- $\tau_{ot}$  = Estimated time to cross each shell

Subscripts

- $c$  = Catastrophic collision
- $d$  = Decaying satellites
- $h$  = Active satellites operating in the  $h^{th}$  altitude shell
- $i, j$  = Subscripts referring to the species of the model
- $nc$  = Non-catastrophic (damaging) collision
- $r$  = Raising satellites

## I. Introduction

In the last years, space activity has rapidly increased. Hundreds of satellites have been launched, and many others are planned. Large constellations have been confirmed to be deployed, causing the number of satellites to increase dramatically. Some examples are the Space-X Starlink constellation, with more than 3000 satellites already in orbit and a potential final number of about 42000 satellites [1], the Amazon Kuiper constellation, with approximately 7800 satellites [2], and Astra Space constellation with 13000 satellites [3]. Such a high number of new launches will affect satellites' safety during orbit transfer maneuvers, for example, from the injection orbit to the operational orbit. Indeed, a satellite can experience in-transit conjunction with other Anthropogenic Space Objects (ASO) and debris. For instance, the Two Line Elements (TLEs) evinced that Starlink satellites are usually launched in batches of 60, which are deployed into an injection orbit; they are then raised to a higher altitude parking orbit before being raised again to the final operative orbit. Assuming that most new constellations follow the same deployment pattern, the number of objects crossing the first shells will be extremely high and dangerous. Therefore, the primary aim of this paper is to incorporate orbit raising and deorbiting maneuvers into a multi-species multi-shells source-sink evolutionary model, calculating the

satellite flux between shells and analyzing their impact on the population's time evolution. To the authors' knowledge, prior source-sink models have not considered the effects of orbit transfer maneuvers. The main novelty here lies in the inclusion of orbit raising and deorbiting, which are time-dependent maneuvers resulting in time-dependent effects, into a model that lacks instantaneous information on orbital elements for each object.

An estimate of the time evolution of the space environment is typically determined using one of the following two methodologies. The first exploits a Monte Carlo (MC) type approach, where all the objects are propagated forward in time. This method typically considers the real physical dynamics of the single object and considers various perturbations, such as atmospheric drag, solar radiation pressure, the oblateness of the Earth, third-body perturbations, and space weather (including solar cycle effects), and in addition, collisions and explosions. Unfortunately, although very accurate, this approach is computationally expensive: to provide general statistics for some critical parameters, many runs are required. Examples of models employing this approach are LEGEND [4], DAMAGE [5], and DELTA [6]. On the other hand, the second methodology relies on the so-called source-sink model, which is a system of coupled Ordinary Differential Equations (ODEs) describing the evolution of different categories of space objects, such as active satellites ( $S$ ), derelicts ( $D$ ), debris ( $N$ ) and rocket bodies ( $B$ ). The main difference concerning MC methods is the lack of information about single objects; in source-sink models, objects are propagated as species. These models, typically called particle-in-a-box models, are computationally lighter and faster, thus proving to be suitable for long-term propagation and sensitivity analyses.

Source-sink models have already been employed to study the LEO population in literature. For example, the model proposed by Talent [7], based on a first-order ODE, describes the evolution trend of the objects in orbit. Somma et al. introduced a feedback controller [8] and developed the so-called MISSD (Model for Investigating control Strategies for Space Debris) [9]. This model has also been exploited by Trozzi et al. [10] to study the evolution of the LEO region and analyze different definitions of space environment capacity, the number-time product [11], and the Criticality of the Spacecraft Index (CSI) [12]. The model used in this work, an evolutionary multi-shell multi-species source-sink model belonging to the MIT Orbital Capacity Assessment Tool (MOCAT) family, which consists of both source-sink and Monte Carlo models, has already been exploited to study and analyze different aspects of the space environment evolution as well as the orbital capacity. D'Ambrosio et al. [13] used the MOCAT-3 to estimate the LEO orbital capacity, the definition of which is based on the stable equilibrium points of the source-sink model. Moreover, Miles et al. [14] and D'Ambrosio et al. [15, 16] developed different versions of MOCAT by considering the effects of orbital slotting and the impacts of untracked debris, respectively. In addition, Jang et al. [17] worked on the stability of the LEO environment and the assessment of the system-level risk in the LEO environment. Finally, Pasiecznik [18] and D'Ambrosio [19] studied the effects of the launch rate distribution on the stability of source-sink models and the sensitivity of LEO environmental capacity to the projected orbital demand and the orbital slotting. The previous MOCAT models lacked the presence of the rocket bodies family, the major potential debris source, and assumed direct injection and removal

of objects. Thus, this work aims to fill these gaps, achieving a more realistic model by including rocket bodies and upwards and downward fluxes of objects due to orbit raise and decay.

The manuscript is structured as follows: it begins with the introduction of the proposed source-sink model, which follows the typical structure of a MOCAT model. This explanation encompasses analyses of various aspects, including new launches, post-mission disposal, collisions, and atmospheric drag flux, while integrating new elements, such as rocket bodies, and refining the categorization of active satellites into raising, operative, and deorbiting satellites, adding depth and precision to the model. A significant focus is placed on the innovative procedure for integrating the flux of objects resulting from orbit transfer maneuvers. Subsequently, the paper presents and compares the results obtained using the proposed model. Additionally, a sensitivity analysis involving fundamental parameters is conducted. Finally, the paper concludes with a summary of key findings and remarks.

## II. Probabilistic Source-Sink Model

The proposed probabilistic source-sink model is a multi-bin multi-species model in which the LEO region is divided into many orbital spherical shells, and different categories of objects are considered. One of the novelties proposed with respect to the previous works is the introduction of the rocket bodies as a new family and the subdivision of active satellites into three subcategories: raising, decaying, and operating satellites. Respectively, they represent the active satellites maneuvering from the injection to the operative orbit, from the operative to the reentry orbit, i.e., altitude lower than 200 km, and those staying in their assigned operative shell. The species taken into account are: active satellites  $S(h, t)$ , derelicts  $D(h, t)$ , debris  $N(h, t)$ , and rocket bodies  $B(h, t)$ . They can be grouped into the following vector

$$\mathbf{P}(h, t) = [S(h, t), D(h, t), N(h, t), B(h, t)] \quad (1)$$

where  $h$  indicates the  $h^{th}$  altitude shell, while  $t$  is the time instant considered. The active satellites can be expressed as

$$\mathbf{S}(h, t) = [S_h(h, t), S_r(h, t), S_d(h, t)] \quad (2)$$

where the subscript  $h$  indicates the active satellites operating in the  $h^{th}$  altitude shell, the subscript  $r$  and  $d$  represents the raising and the decaying satellites. The three satellite families share the same physical characteristics and have the capability to maneuver. Be aware that, from now on, both the arguments  $(h, t)$  will be omitted for a lighter notation, even if the dependence remains.

The current MOCAT model considers the following assumptions:

- i Only near-circular orbits with an altitude between 200 km and 2000 km are considered. Concerning the present LEO population derived from the TLEs, over 90% of objects exhibit an eccentricity lower than 0.1.

- ii The atmosphere is considered static and spherical symmetry of the Earth's gravitational potential is assumed. The model relies exclusively on radial information for objects and does not possess data regarding the position and velocity of each object at each time instant. As a result, Earth harmonics, third-body effects, and Solar Radiation Pressure (SRP) cannot be modeled. The only perturbation taken into account is atmospheric drag, which means that the only orbital element undergoing change is the semi-major axis, denoted as  $a$ .
- iii Active satellites are expected to perform station-keeping maneuvers, enabling them to counteract the effects of atmospheric drag.
- iv No active debris removal is considered. The only natural sink to reduce the population of space objects is the atmospheric drag.
- v The minimum size of debris able to disrupt a satellite is 10 cm, which is also the the nominal sensitivity limit of the U.S. Space Surveillance Network [20]. This assumptions has been frequently used in literature, for instance in Refs. [9, 10].
- vi Explosions are not included into the computation of the results due to the assumption that technology will advance in the future. However, they may be considered in future research studies.

With respect to the previous MOCAT models, two main assumptions are dropped: firstly, new active satellites can be instantaneously injected into their final operative altitude, or they can be launched into a parking orbit and undergo orbit raising maneuvers; and secondly, after the mean satellite lifetime ( $\Delta t$ ), active satellites are no longer directly removed with a certain probability of success, but they will decrease their semi-major axis through deorbiting maneuvers. Therefore, flows of objects from lower to upper shells, and vice-versa, are now modelled. A schematic representation of the model is visible in Fig. 1. Active satellites, rocket bodies, and derelicts constitute intact objects. Collisions, represented by dashed black arrows, could involve objects from the same or different species, giving rise to derelicts and debris or debris only. Moreover, derelicts might be created from each category composing active satellites. These transitions are indicated with the dotted red arrows and will be explained in Section II.E. For what concerns active satellites, both  $S_r$  and  $S_h$  are launched, represented by green arrows, while the category transitions among the  $S$  families and the flow between different shells are indicated with  $\vartheta$ . Let the model considering  $P = [S_h, S_r, S_d, D, N, B]$  be referred to as the MOCAT-6RD, where '6' represents the number of species involved, and 'RD' indicates that orbit raising and deorbiting maneuvers are included. The model without decaying satellites  $S_d$  is named MOCAT-5R, with '5' as the species involved and 'R' signifying that orbit raising is modeled (the 'D' is omitted as deorbiting is not included). Lastly, the simplified model lacking orbit transfer flux is named MOCAT-4B, with four species included, denoted as  $P = [S, D, N, B]$ . Here, 'B' represents rocket bodies and serves to distinguish this model from other MOCAT models that also have four species but exclude rocket bodies.

The evolution in time of the population  $\mathbf{P}$  is captured by a system of ordinary differential equations, written in a

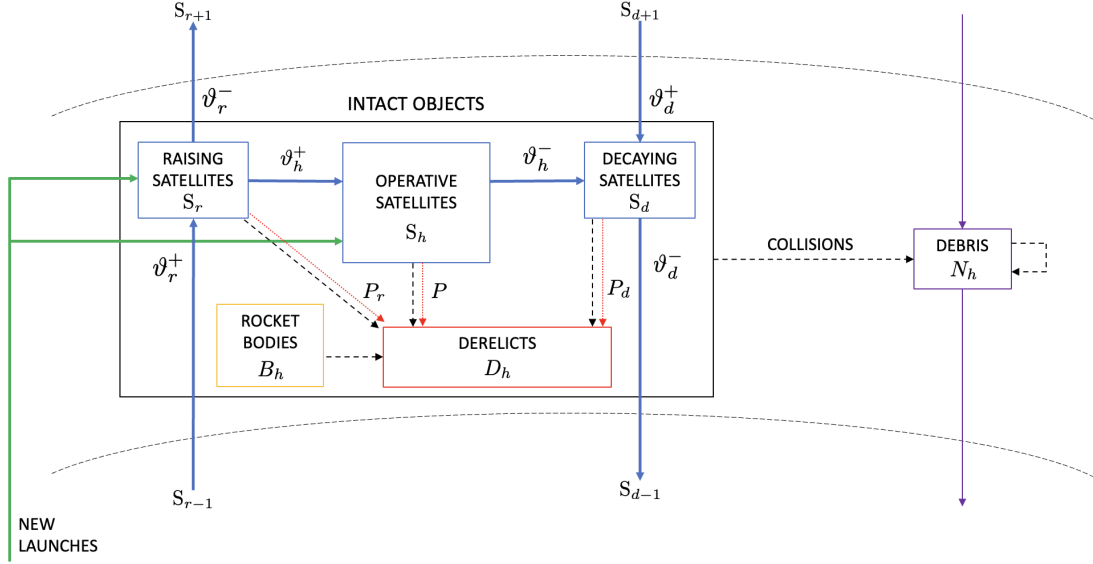


**Fig. 1 Schematics of the MOCAT-6RD source-sink model.**

vectorial form as

$$\dot{P} = \dot{\Lambda} + \dot{C}_{PMD} + \dot{C} + \dot{F} \quad (3)$$

where  $\dot{\Lambda}$  represents a term related to new launches,  $\dot{C}_{PMD}$  to Post-Mission Disposal (PMD),  $\dot{C}$  and  $\dot{F}$  to collisions and other additional fluxes respectively. The unit of Eq. (3) is number of objects per year [# / year]. Let us analyze the terms in more detail.

### A. New Launches

The variable  $\dot{\Lambda}$  is the launch rate, it indicates the number of objects launched per year. It can be expressed as

$$\dot{\Lambda} = [\lambda_{S_h}, \lambda_{S_r}, \lambda_{S_d}, \lambda_D, \lambda_N, \lambda_B] \quad (4)$$

where  $\lambda_i$  is the launch rate for object of type  $i$ . Since decaying satellites, derelicts, and debris are not launched, the corresponding  $\lambda$  is equal to zero. Furthermore, the model assumes that all future rocket bodies used to inject active satellites will be reusable and will reenter after launch, thus  $\lambda_B = 0$ . Particular attention needs to be paid to the first two terms. International Telecommunication Union's (ITU) files are used for this purpose. The list comprises a series of entries providing the operator's name, the orbital elements, and the number of satellites planned to be launched. To use these data, the following assumptions are made:

- i Rwanda satellites, present with more than 300,000 objects, are not considered feasible and thus removed.
- ii The list is filtered according to the altitude range (200-2000 km) and the eccentricity (near-circular orbits).

- iii To the remaining satellites, a confidence level is given, and a percentage is considered.
- iv A deployment time of 10 years is assumed. During these years, the number of satellites launched follows the exponential trend extrapolated from historical data. After 10 years, the number of satellites remains constant.
- v List entries with more than 50 satellites are considered constellation satellites. Those are then binned into parking orbits and will undergo orbit raising. The remaining satellites are directly injected into their operative orbits.

Historical data are used to extrapolate the number of satellites that might be launched in the near future. To this aim, the entire Space-Track catalog was downloaded and utilized to retrieve the number of satellites launched yearly from the beginning of space exploration until November 2022. As shown in Figure 2(a), the number of objects is drastically increasing, and an exponential function can fit the trend. Moreover, Space-Track was also used to retrieve the entire set of Starlink's and OneWeb's TLEs, from which the distribution of injection orbits was recovered. According to Figure 2(b), most Starlink satellites are launched between 200 km and 300 km, while OneWeb between 400 km and 500 km. Therefore, for future launches, two injection orbits are used: satellites with an operative orbit between 200 km and 400 km are injected into the first shell at an altitude of 250 km, while those designated for higher altitudes are launched at 450 km. The exponential function fitting the historical data is utilized to scale up the number of satellites launched annually. Thus, combining the ITU's file with historical data information makes it possible to compute the future launch profile. In Figures 3(a) and 3(b) the number of satellites composing the launch profile  $\lambda_{S_r}$  and  $\lambda_{S_h}$  are reported. Another step must be taken concerning the distribution on the left, the one associated with raising satellites. The satellites are grouped into two batches and are inserted in the model at the two injection orbits aforementioned. Finally, note the numbers reported in the legends of Figure 3: these values represent the number of satellites that would be launched according to ITU's files and the exponential trend. It would mean that more than one thousand satellites per day would need to be launched, which is assumed to be unfeasible with the current level of technology. Therefore, those numbers reported are further reduced by a factor of 10.

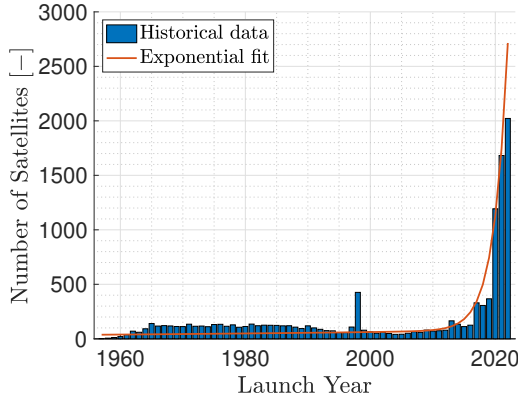
## B. Post-Mission Disposal

The Post-Mission Disposal takes only into account the mean operational lifetime of the satellite,  $\Delta t$ . At the end of their lifetime, a percentage of active satellites is assumed to fail to conduct PMD, consequently becoming derelict, while the remaining switch from operating satellites  $S_h$  to decaying satellites  $S_d$ . As a result, the term  $\dot{C}_{PMD}$  is

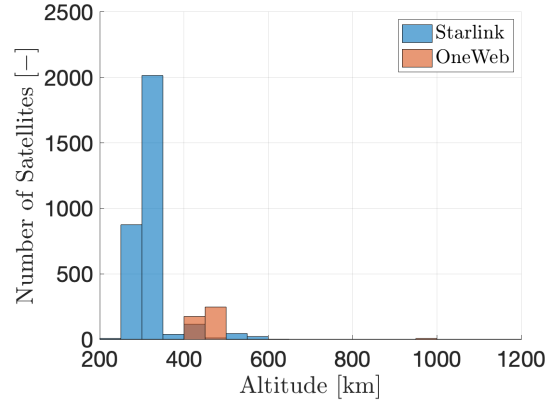
$$\dot{C}_{PMD} = [-\vartheta_h^- S_h, 0, +P_m \vartheta_h^- S_h, +(1 - P_m) \vartheta_h^- S_h, 0, 0] \quad (5)$$

---

<sup>†</sup>The aim is to reproduce Figure 2.8 of the ESA's annual space environment report [21].

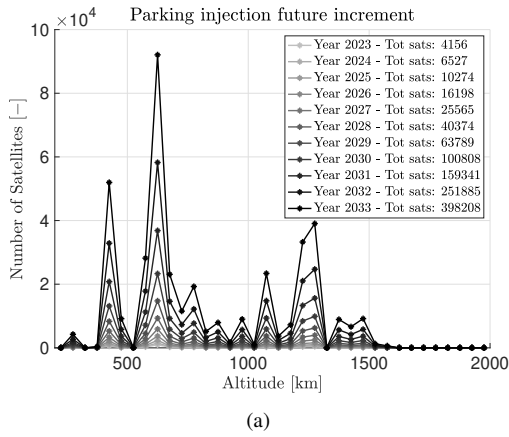


(a) Number of satellites launched per year in LEO according to Space-Track catalog.<sup>†</sup>

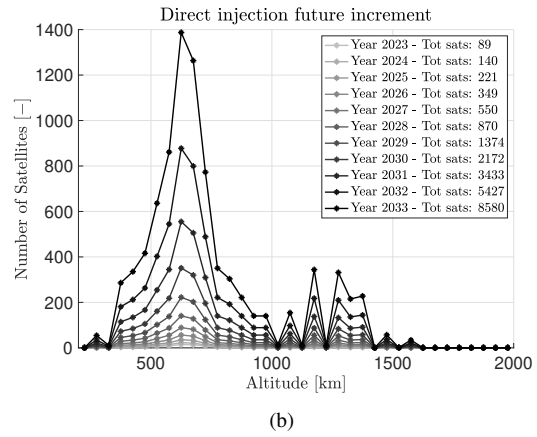


(b) Starlink's and OneWeb's satellites parking orbit analysis.

**Fig. 2** Historical data and TLEs analysis to extrapolate the future launch profile and determine the injection orbits.



(a)



(b)

**Fig. 3** Future extrapolation of the number of satellites launched according to the ITU's files with 80% confidence level.

where  $P_m$  is defined as the post-mission disposal probability of success and

$$\vartheta_h^- = \frac{1}{\Delta t} \quad (6)$$

represents the PMD transition. The first component in Eq. (5) is negative because operating satellites are removed from the population  $S_h$ . A percentage of those who fail the disposal are added to the derelicts  $D$ , whereas the remaining successfully begin decaying maneuvers and are added to  $S_d$ .

### C. Collision

Collisions are modeled according to the kinetic theory of gases; this approach has already been used in previous works [8, 10, 13]. The collision interactions can be simplified by first summing all active satellites in a specific shell, where  $S = S_h + S_r + S_d$ . Note that  $S$  is different from  $\mathcal{S}$ : the first represents an  $[n \times 1]$  vector, where  $n$  is the number of shells, while the second is a  $[n \times 3]$  matrix. All active satellites are assumed to have the same collision avoidance capability, regardless of their current operational phase (raising, station keeping, or deorbiting). The collisions term  $\dot{C}$  can be written as

$$\dot{C} = [\dot{C}_S, \dot{C}_D, \dot{C}_N \cdot n_f, \dot{C}_B] \quad (7)$$

where  $n_f$  is the number of fragments generated by a collision, estimated with the NASA standard breakup models [20]. According to this model, two different kinds of collisions are considered: catastrophic  $n_{f,c}$  and non-catastrophic  $n_{f,nc}$ . This analysis assumes that all the collisions involving active satellites, derelicts, and rocket bodies are catastrophic, whereas those involving debris are non-catastrophic. The main reason is related to the ASO physical characteristic assigned, reported in Table 5. Table 1 explicitly indicates all the combinations among the species.

**Table 1 Collision classification between the species.**

Species	S	D	N	B
S	$n_{f,c}$	$n_{f,c}$	$n_{f,nc}$	$n_{f,c}$
D	$n_{f,c}$	$n_{f,c}$	$n_{f,nc}$	$n_{f,c}$
N	$n_{f,nc}$	$n_{f,nc}$	$n_{f,nc}$	$n_{f,nc}$
B	$n_{f,c}$	$n_{f,c}$	$n_{f,nc}$	$n_{f,c}$

The number of fragments generated by the collision between object  $i$  and object  $j$  can be calculated using [20]

$$n_f = \begin{cases} 0.1 L_C^{-1.71} (M_i + M_j)^{0.75} & \text{catastrophic} \\ 0.1 L_C^{-1.71} (M_p \cdot v_{imp}^2)^{0.75} & \text{non-catastrophic} \end{cases} \quad (8)$$

where  $L_C$  is the characteristic length of the minimum size of generated debris (assumed to be 0.1 m),  $M_{i,j}$  is the mass associated with the objects  $i, j$ , instead  $M_p = \min(M_i, M_j)$  is the mass of the projectile (i.e., the mass of the less massive object), and finally  $v_{imp}$  is the impact velocity assumed to be equal to 10 km/s. While  $v_{imp}$  varies with altitude, it can be reasonably approximated according to Ref. [9] as  $v_{imp} = \sqrt{2}v_c(h)$ , where  $v_c(h)$  represents the orbital velocity at the midpoint of the corresponding shell. To provide context, if a circular orbit is used as a reference,  $v_{imp}$  would range from 11 km/s at an altitude of 200 km to 9.75 km/s at an altitude of 2000 km. It's worth noting that an average velocity of 10 km/s is commonly employed in low Earth orbit scenarios [7, 9, 22], which is also the approach adopted in this study.

Indicating with  $Q_i$  one among the  $N_s$  species considered ( $N_s = 4$ ), the terms composing Eq. (7) can be written as

$$\dot{C}_i = \sum_{j=1}^{N_s} \Gamma_{i,j} \phi_{i,j} Q_i Q_j + \dot{C}_{i,add} \quad (9)$$

When considering a species  $Q_i$ , the first term in Eq. (9) accounts for the net gain or loss in the number of objects resulting from collisions directly involving species  $Q_i$ . The symbol  $\dot{C}_{i,add}$  is a compact way to represent the change in species  $Q_i$  caused by collisions that are not directly related to species  $Q_i$ . The matrix  $\Gamma_{i,j}$  collects the coefficients related to collision avoidance probability and the derelict generation, namely

$$\Gamma = \begin{bmatrix} -\alpha_a & -(\delta + \alpha) & -(\delta + \alpha) & -(\delta_B + \alpha) \frac{S}{B+S} \\ +\delta & -1 & -1 & +\delta_B \\ +\alpha & +1 & +1 & +1 \\ -(\delta_B + \alpha) \frac{B}{B+S} & -(1 + \delta_B) & -(1 + \delta_B) & -(1 + \delta_B) \end{bmatrix} \quad (10)$$

where  $\delta$  and  $\delta_B$  are the ratios of the density of disabling to lethal debris, while  $\alpha$  and  $\alpha_a$  the fractions of collisions that a live satellite fails to avoid ( $\alpha_a$  is used for  $S$ - $S$  collision). It is assumed that the coefficient related to the generation of derelicts involving satellites ( $\delta$ ) is equal to the coefficient involving rocket bodies ( $\delta_B$ ). It can be highlighted that the signs in Eq. (10) indicates if the corresponding quantity is added or removed from the species. In fact, the third row related to debris has all positive signs since every collision generates debris. By substituting  $S$  with the three subcategories, it is possible to expand the equation and write the explicit relation for each term  $S_h$ ,  $S_r$ , and  $S_d$ .

The  $\dot{C}_{i,add}$  contributions are determined by substituting the subscript  $i$  with one of the four species labels:  $s, d, n, b$ , corresponding to the four distinct species:

$$\begin{cases} \dot{C}_{s,add} = 0 \\ \dot{C}_{d,add} = +\phi_{s,n}\delta NS + \phi_{s,b}\delta_B BS + \phi_{n,b}\delta_B NB + \phi_{b,b}\delta_B B^2 \\ \dot{C}_{n,add} = \alpha_a \phi_{s,s} S^2 + \phi_{s,d}\alpha SD + \phi_{s,b}\alpha SB + \phi_{d,d} D^2 + \phi_{d,b} DB + \phi_{b,b} B^2 \\ \dot{C}_{b,add} = 0 \end{cases} \quad (11)$$

It is important to emphasize that there are no collision scenarios that generate new active satellites and rocket bodies.

Finally, the last component to be addressed is the probability of collision  $\phi_{i,j}$ , between objects  $i$  and  $j$ . According to references [9, 10], it can be expressed as

$$\phi_{i,j} = \pi \frac{v_{imp} \sigma_{i,j}}{V(h)} \quad (12)$$

where  $v_{imp}$  and  $V(h)$  are the impact velocity, assumed constant, and the volume of the altitude bin involved, respectively. Instead,  $\sigma_{i,j}$  represents the impact parameter between the two species and is calculated based on references [9, 10] as

$$\sigma_{i,j} = (r_i + r_j)^2 \quad (13)$$

with  $r_{i,j}$  being the radius of the colliding objects.

#### D. Atmospheric Drag Flux

The flux of objects decaying into lower altitude shells due to the atmospheric drag is indicated as  $\dot{F}_d$  and it can be expressed as

$$\dot{F}_d = [0, \dot{F}_{d,D}, \dot{F}_{d,N}, \dot{F}_{d,B}] \quad (14)$$

All the families, except for active satellites, supposed to be capable of performing station-keeping maneuvers, are subjected to this flux. The atmospheric drag flux affecting species  $Q$ , results in

$$\dot{F}_{d,Q} = -\frac{Q_+ v_+}{d} + \frac{Qv}{d} \quad (15)$$

where the subscript + denotes the upper shell, while its absence indicates the current shell. The parameter  $d$  indicates the thickness of both the upper and current orbital shells, assumed to be equal for spherical shells. The variable  $v = \dot{a}$  represents the rate of change in semi-major axis due to atmospheric drag. Therefore, the fraction  $d/v$  signifies the time an object spends in a specific shell due to drag effects [9, 10]. In Eq. (15), the first term accounts for the influx of objects entering the current shell, while the second term represents the outflux of objects leaving the current shell. By combining specific orbital energy and the conservation of specific angular momentum under the influence of drag alone [9], the parameter  $v$  can be approximated as:

$$v = -\rho B_c \sqrt{\mu R} \quad (16)$$

with  $\mu$  being the Earth's gravitational parameter and  $\rho$  the atmospheric density at a radial distance  $R$ . In the above equation, the species-dependent ballistic coefficient  $B_c$  is computed using

$$B_c = c_D \frac{A}{m} \quad (17)$$

where  $c_D$  is the drag coefficient,  $A$  and  $m$  the area and the mass of the object. The static exponential density profile derived from CIRA-72 (Committee on Space Research International reference Atmosphere) is used in this work [23].

The altitude-dependent density is

$$\rho = \rho_0 \exp\left(-\frac{h - h_0}{H}\right) \quad (18)$$

where  $\rho_0$  is the atmospheric density at the reference altitude  $h_0$ ,  $H$  is the scale height, and  $h$  is the altitude considered. Table 8-4 of reference [23] presents the reference values considered. However, due to its simplicity, this model does not consider many external factors, such as geomagnetic storms and solar activity, which can strongly affect the density. Indeed, those effects can be taken into account by performing an atmospheric density adjustment to have a piecewise-continuous formulation with a mean solar activity [23]. Therefore, the height scale is considered a function of the exospheric temperature (i.e., the asymptotic value of the temperature reached at a higher altitude of the exosphere), which in turn depends on the F10.7 solar flux index [13, 16]. Nevertheless, solar activity and geomagnetic storms cause frequent and significant changes over time in the atmospheric density. The Jacchia-Bowman 2008 (JB2008) [24], a time-varying atmospheric model, is able to capture these dynamics. It has been validated by comparing its predictions to actual daily density drag data from satellites in orbit, and has demonstrated significant improvement over previous density models. The JB2008 is the current standard for predicting thermospheric mass density. Despite JB2008 typically depends on longitude and latitude, which is not information accessible with source-sink models, a dataset is precomputed on a spatial-temporal grid using the approach in Ref. [16]. During the propagation of the MOCAT models, interpolation techniques are used to determine the atmospheric density at a specific time and altitude based on this precomputed data. A comparison between the static exponential and the Jacchia-Bowman 2008 model is reported in Section III.D.

### **E. Orbit Transfer Flux**

As already stated, an important novelty introduced in this work is the flux of objects related to orbit transfer maneuvers, which can include both orbit raising and deorbit maneuvers. The first ones are related to the new satellites launched into space that are transitioning to a higher final orbit. On the contrary, deorbit maneuvers are required at the end of a satellite's life to reduce the orbit's altitude to a region where the spacecraft are burned up in the atmosphere during reentry: less than 200 km. While PMD was often considered in previous models as a percentage level of compliance with the post-mission disposal guidelines (the satellites are assumed to be instantly removed from their altitude shell), its temporary effects related to the flux of objects passing through different shells are often neglected. At the same time, the assumption behind the launch rate is that objects instantly reach their final altitude as soon as they are launched. Indeed, this paper achieves a higher fidelity model by including the flux of objects passing through higher altitude orbital shells (for the case of orbit raising) and lower altitude orbital shells (for the case of deorbit). In fact, the fluxes of objects related to orbit transfer maneuvers lead to a temporary increase in the population associated with each shell and, thus, a higher probability of collision and debris creation.

The orbit transfer flux is modeled by considering the semi-major axis secular variation and its rate of change under a low-thrust continuously applied control  $f$ . As indicated by Di Carlo and Vasile [25], it can be expressed in a

radial-transverse-normal RTN reference frame as

$$\mathbf{f} = \begin{bmatrix} f_R \\ f_T \\ f_N \end{bmatrix} = \begin{bmatrix} \epsilon \cos(\beta) \sin(\alpha) \\ \epsilon \cos(\beta) \cos(\alpha) \\ \epsilon \sin(\beta) \end{bmatrix} \quad (19)$$

with  $\epsilon$  indicating the magnitude of the constant low-thrust acceleration,  $\alpha$  the azimuth angle formed with the transverse direction, and  $\beta$  the elevation angle with respect to the orbit plane. The study examines the thrust angles that yield the maximum instantaneous rate of change of the orbital elements by computing the first derivatives of Gauss' equations with respect to  $\alpha$  and  $\beta$ . The analysis indicates that the maximum rate of change of the semi-major axis occurs when thrust is applied in a planar direction ( $\beta = 0$ ) and the azimuth angle equals the flight path angle  $\gamma$ , which means that the spacecraft always provides the control acceleration along the velocity direction. Specifically,  $\alpha = \gamma$  results in an increase in the semi-major axis, while  $\alpha = \pi + \gamma$  leads to a decrease. The assumption of low-thrust acceleration yields in a long spiral trajectory, where perturbations over a single orbital period are negligible. This spiral path causes satellites to spend considerable time in different shells before reaching their final altitude, while maintaining a low mean eccentricity during the transfer, which aligns with the MOCAT assumptions.

According to Di Carlo and Vasile [25], the semi-major axis secular variation as a function of time  $\bar{a}(t)$  can be expressed as follows:

$$\bar{a}(t) = \left[ \frac{1}{\bar{a}_0} + C_1 t^2 - C_2 t \right]^{-1} \quad (20)$$

with  $\bar{a}_0$  being the initial value of the semi-major axis secular variation (in this work, approximately set equal to the initial parking orbit altitude). The coefficients  $C_1$  and  $C_2$  are provided by:

$$C_1 = \left( \frac{\epsilon(1 - \bar{e}^2)f(\bar{e})}{2\pi\sqrt{\mu}} \right)^2 \quad (21)$$

$$C_2 = \text{sgn}(\cos \alpha) \frac{\epsilon(1 - \bar{e}^2)f(\bar{e})}{\pi\sqrt{\bar{a}_0\mu}} \quad (22)$$

where  $\bar{e}$  is the mean value of the eccentricity,  $\text{sgn}(\cdot)$  indicates the sign function, and  $f(\bar{e})$  is represented by:

$$f(\bar{e}) = \frac{2}{1 - \bar{e}} E_{Ic} \left( \frac{4\bar{e}}{(1 + \bar{e})^2} \right) + \frac{2}{1 + \bar{e}} F_{Ic} \left( \frac{4\bar{e}}{(1 + \bar{e})^2} \right) \quad (23)$$

where  $F_{Ic}$  and  $E_{Ic}$  are the complete elliptic integrals of the first and second kind, respectively:

$$F_{Ic}(q) = F_I\left(\frac{\pi}{2}, q\right) \quad (24)$$

$$E_{Ic}(q) = E_I\left(\frac{\pi}{2}, q\right) \quad (25)$$

The proposed approach relies on the time spent by the satellites within each shell during the orbit transfer maneuvers, i.e., the time required to reach the above (or below) shell from the current one. An estimation of this residence time  $\tau_{ot}(h) = [\tau_{ot_1}, \dots, \tau_{ot_n}]$  can be computed by inverting Eq. (20) and setting  $\bar{a}_f = \bar{a}_{h+1}$  and  $\bar{a}_0 = \bar{a}_h$ . It is worth noticing that  $\tau_{ot}$  is altitude dependent, and, in particular, the higher the altitude shell, the lower the time required to cross it. Let us also define

$$\mathbf{T} = \begin{bmatrix} \tau_{ot_1} & & \\ & \ddots & \\ & & \tau_{ot_n} \end{bmatrix} \quad (26)$$

Once the raising satellites are injected into the parking orbits, they start to increase their altitude. Whenever the launched batch switches from the current to the upper shell, a certain number of satellites (i.e., those whose final operational altitude is within the current shell) are deposited. This phenomenon is represented by the transition from the  $S_r$  to the  $S_h$  family, and it is described by the diagonal matrix

$$\mathbf{\Theta}_h^+ = \begin{bmatrix} \vartheta_{h_1}^+ & & \\ & \ddots & \\ & & \vartheta_{h_n}^+ \end{bmatrix} \quad (27)$$

Each element of the matrix  $\vartheta_h^+$  represents the fraction of dropped satellites over the number of satellites still raising. Thus, each component is altitude dependant. The matrix is a  $[n \times n]$  matrix.

The satellites that are still raising need to transition from the current to the upper shell, while those left behind have to be removed from the population of the current shell. The following two matrices capture this dynamic:

$$\mathbf{\Theta}_r^+ = \begin{bmatrix} 0 & & & \\ (1 - \vartheta_{h_1}^+) & 0 & & \\ & \ddots & \ddots & \\ & & (1 - \vartheta_{h_{n-1}}^+) & 0 \end{bmatrix} \quad \mathbf{\Theta}_r^- = \begin{bmatrix} (1 - \vartheta_{h_1}^+) & & & \\ & \ddots & & \\ & & & (1 - \vartheta_{h_n}^+) \end{bmatrix} \quad (28)$$

Notice that  $\Theta_r^+$  is a lower triangular matrix. Moreover, whenever a shell is associated with an injection orbit, the corresponding entries are zeros. Indeed, there is no transitioning flow of raising satellites for those shells.

Once the satellites reach the end of life, they have to start the PMD, which corresponds to the transition from operating to decaying satellites already taken into account in Eq. (5). However, analogously to raising, each shell is also subject to the decaying flow: satellites, starting from the uppermost shell, start lowering their altitude until reenter. Satellites leaving the current shell can be represented by  $\Theta_d^-$ , whereas those entering are expressed through  $\Theta_d^+$ , and result to be

$$\Theta_d^+ = \begin{bmatrix} 0 & 1 & & & \\ & & \ddots & \ddots & \\ & & & 0 & 1 \\ & & & & 0 \end{bmatrix} \quad \Theta_d^- = \begin{bmatrix} 1 & & & \\ & \ddots & & \\ & & & 1 \end{bmatrix} \quad (29)$$

Also, in this case, the resulting matrices are  $[nxn]$  squared. Moreover,  $\Theta_d^+$  is an upper triangular matrix, while  $\Theta_d^-$  is diagonal.

It is now possible to express the terms composing the orbit transfer flow as

$$\dot{F}_{ot,S_h} = \Theta_h^+ \mathbf{T}^{-1} S_r \quad (30)$$

$$\dot{F}_{ot,S_r} = -\Theta_h^+ \mathbf{T}^{-1} S_r + \Theta_r^+ \mathbf{T}^{-1} S_r - \Theta_r^- \mathbf{T}^{-1} S_r - (1 - P_r) \mathbf{T}^{-1} S_r \quad (31)$$

$$\dot{F}_{ot,S_d} = P_m \Theta_h^- \mathbf{T}^{-1} S_h - \Theta_d^- \mathbf{T}^{-1} S_d + \Theta_d^+ \mathbf{T}^{-1} S_d - (1 - P_d) \mathbf{T}^{-1} S_d \quad (32)$$

Another novelty of the current model is the presence of the term  $(1 - P_{r,d}) \mathbf{T}^{-1} S_{r,d}$  in both Eqs. (31) and (32). This term models the possibility of failure during orbit transfer maneuvers, e.g., propulsion system failure or propellant depletion. In particular,  $P_{r,d}$ , similarly to  $P_m$ , are defined as the probability of successful completion of raising and deorbit, respectively. Whenever a failure occurs, a fraction of  $S_r$  and  $S_d$  is removed and added to the derelicts

$$\dot{F}_{ot,D} = (1 - P_r) \mathbf{T}^{-1} S_r + (1 - P_d) \mathbf{T}^{-1} S_d \quad (33)$$

Finally, it is possible to express the flux as

$$\dot{F}_{ot} = [\dot{F}_{ot,S_h}, \dot{F}_{ot,S_r}, \dot{F}_{ot,S_d}, \dot{F}_{ot,D}, 0, 0] \quad (34)$$

The orbit transfer flux is thus summed to the atmospheric drag flux to compute the total flux affecting the source-sink

model species

$$\dot{F} = \dot{F}_{ot} + \dot{F}_d \quad (35)$$

To sum up, the primary sources, sinks, and interactions are explicitly reported in the following tables. In particular, Table 2 reports the terms involving active satellites, while Table 3 summarises all the species, where  $S = S_h + S_r + S_d$ .

**Table 2 Interactions among the active satellites of the MOCAT-6RD model.**

	Species	$S_h$ (operating satellites)	$S_r$ (raising satellites)	$S_d$ (deorbiting satellites)
New launches $\dot{\Lambda}$	--	$\lambda_{S_h}$	$\lambda_{S_r}$	0
Post-Mission Disposal $\dot{C}_{PMD}$	--	$-\vartheta_h^- S_h$	0	$+P_m \vartheta_h^- S_h$
Orbit transfer Fluxes $\dot{F}$	--	$\dot{F}_{ot,S_h}$	$\dot{F}_{ot,S_r}$	$\dot{F}_{ot,S_d}$
	$S_h$	$-\alpha_a \phi_{s,s} S_h^2$	$-\alpha_a \phi_{s,s} S_h S_r$	$-\alpha_a \phi_{s,s} S_h S_d$
Collisions sources $\dot{C}$	$S_r$	$-\alpha_a \phi_{s,s} S_r S_h$	$-\alpha_a \phi_{s,s} S_r^2$	$-\alpha_a \phi_{s,s} S_r S_d$
	$S_d$	$-\alpha_a \phi_{s,s} S_d S_h$	$-\alpha_a \phi_{s,s} S_d S_r$	$-\alpha_a \phi_{s,s} S_d^2$

**Table 3 Interactions among the species of the MOCAT-6RD model.**

	Species	$S$ (active satellites)	$D$ (derelicts)	$N$ (debris)	$B$ (rocket bodies)
New Launches $\dot{\Lambda}$	--	$\lambda_S$	0	0	0
Post-Mission Disposal $\dot{C}_{PMD}$	--	$-(1 - P_m) \vartheta_h^- S_h$	$(1 - P_m) \vartheta_h^- S_h$	0	0
Fluxes $\dot{F}$	--	$\dot{F}_{ot,S}$	$\dot{F}_{ot,D} + \dot{F}_{d,D}$	$\dot{F}_{d,N}$	$\dot{F}_{d,B}$
	$S$	$-\alpha_a \phi_{s,s} S^2$	$\phi_{s,d} \delta DS$ $+\phi_{s,n} \delta NS$ $+\phi_{s,b} \delta_B BS$	$n_{f,ss} \alpha_a \phi_{s,s} S^2$ $+n_{f,sd} \phi_{s,d} \alpha SD$ $+n_{f,sn} \phi_{s,n} \alpha SN$ $+n_{f,sb} \phi_{s,b} \alpha SB$	$-\phi_{s,b} (\alpha + \delta_B) \frac{B^2 S}{B + S}$
Collision Sources $\dot{C}$	$D$	$-\phi_{s,d} (\delta + \alpha) SD$	$-\phi_{d,d} D^2$	$n_{f,dd} \phi_{d,d} D^2$ $+n_{f,dn} \phi_{d,n} DN$ $+n_{f,db} \phi_{d,b} DB$	$-\phi_{d,b} (1 + \delta_B) BD$
	$N$	$-\phi_{s,n} (\delta + \alpha) SN$	$-\phi_{d,n} DN$	$n_{f,nn} \phi_{n,n} N^2$	$-\phi_{n,b} (1 + \delta_B) BN$
	$B$	$-\phi_{s,b} (\delta_B + \alpha) \frac{S^2 B}{B + S}$	$\phi_{d,b} \delta_B DB$ $+\phi_{n,b} \delta_B NB$ $+\phi_{b,b} \delta_B B^2$	$n_{f,nb} \phi_{n,b} NB$ $+n_{f,bb} \phi_{b,b} B^2$	$-\phi_{b,b} (1 + \delta_B) B^2$

### III. Numerical simulations

The evolution of the future satellites and debris population, together with the LEO orbital capacity, will be analyzed and compared with other approaches in the literature, highlighting similarities and differences. Some differences are expected due to the additional terms within the model, which have not been considered before.

#### A. Initial Population

The current LEO population is taken as the initial population. From the Space-Track [26] Two Line Elements catalog (as of September 2022) it is possible to retrieve a total of around 24,000 objects. Since the source-sink model is based on different classes, it is important to distinguish the space objects within the four species. To this aim, two other sources have been used: DISCOSweb [27], developed by the European Space Agency, and CelesTrak [28]. The

object class and the status of the objects (active or inactive) are retrieved respectively from the two sources. The MIT's processed catalog consists of 21,014 TLEs, out of which 10,869 are debris, 7,015 payloads (5,129 active and 1,886 inactive), 1,421 rocket bodies, and the remaining 1,709 Mission Related Objects. Figure 4 shows the resulting initial population with respect to the altitude shells.

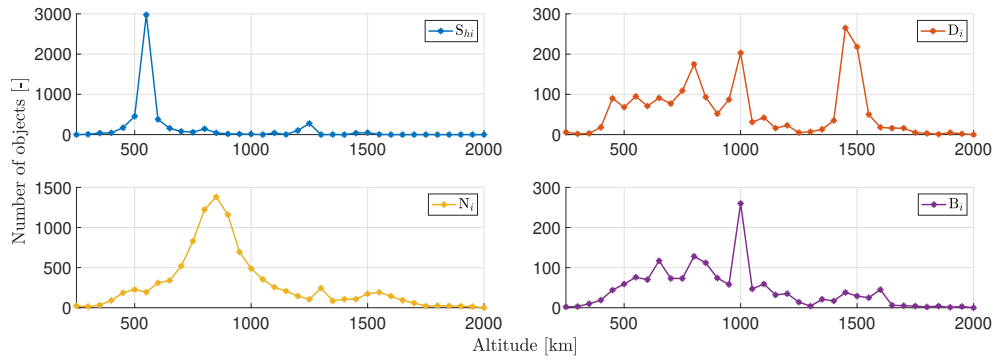


**Fig. 4 Initial population of the model according to MIT's catalog.**

## B. Low-thrust Acceleration Magnitude

One key parameter for both orbit raising and decay is the magnitude of the low-thrust acceleration  $\epsilon$  provided by the propulsion system. The value used in the simulations is determined by analyzing the most recent Starlink and OneWeb TLE database. It is possible to solve Eq. (20) to obtain  $\epsilon$  by providing the initial and final altitude values and the time required for the maneuver. The resulting value is  $\epsilon = 5.0 \cdot 10^{-8} \text{ km/s}^2$ . Figure 5 shows the real time evolution of the altitude, derived from the semi-major axis provided by the TLEs, and the analytical one. Note that once injected, the satellites do not perform orbit transfer maneuvers from the beginning until the operative altitude. Indeed, some time is spent at the same altitude to perform sensor checking and maneuvers to match the desired operative orbit in terms of all the orbital elements, not just the altitude.

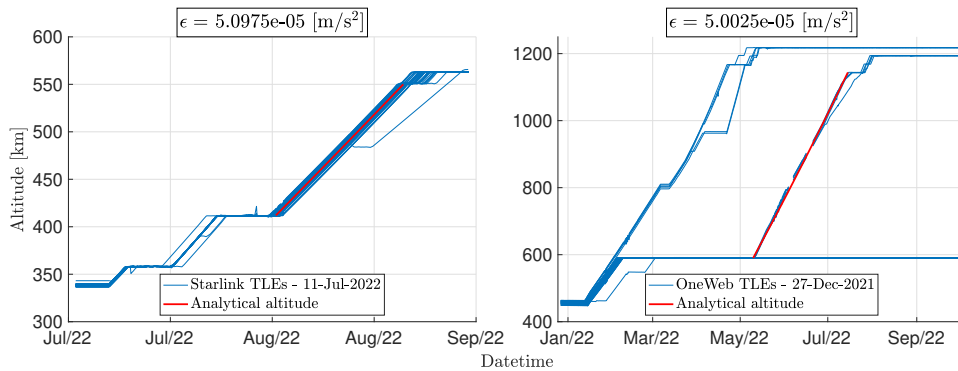


**Fig. 5 Starlink's and OneWeb's TLEs real and analytical altitude evolution in time.**

The acceleration magnitude plays a crucial role in the model. Indeed, each element of the vector  $\tau_{ot}(h)$ , and consequently of the matrix  $\mathbf{T}$  appearing in the orbit transfer flux terms, represents the time spent in each altitude shell while maneuvering. The lower the thrust, the higher the time and the higher the collision probability. With the considered acceleration level,  $\tau_{ot}$  varies from around 7 days (low altitudes) to almost 5 days (high altitudes).

### C. Validation Case

As a first case study, it is worth understanding if the raising mechanism correctly transitions the satellites from  $S_r$  to  $S_h$ . To this aim, it is possible to turn off all the interactions between species and not consider decaying satellites, thus using the MOCAT-5R model. Figure 6 shows the active operational satellites  $S_h$ , indicated as  $S_{\text{raising}}$ , compared to the active satellites population  $S_{\text{no raising}}$ , obtained with MOCAT-4B. The graph compares the population at the end of the propagation time, which is 30 years. As can be seen, the two models achieve the same final desired satellite

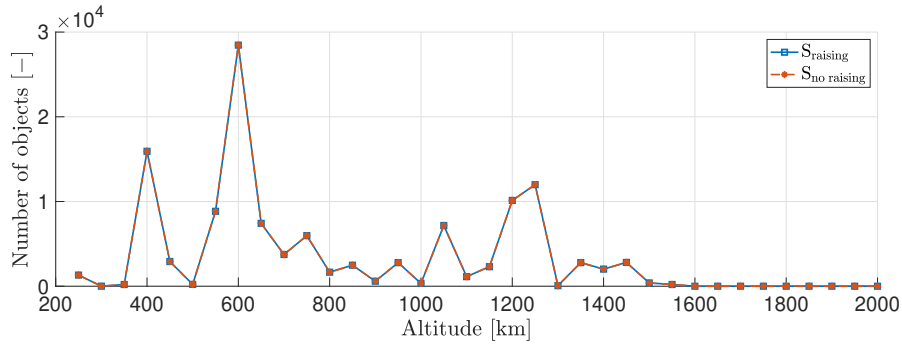


**Fig. 6 Active satellites at the final time without interactions for both raising (MOCAT-5R) and non-raising case (MOCAT-4B).**

distribution. It can also be noticed that the profile resembles the number of satellites launched visible in Figure 3. The good match between the launch profile and the final population is mainly due to the absence of interactions, which prevents collisions from occurring.

### D. Results Comparison

In the following section, results from different MOCAT models are presented. Particular attention is given to the time evolution at different altitudes of the population and to the number of collision events involving the different species. Finally, a sensitivity analysis of the ITU's confidence level and the low-thrust acceleration magnitude  $\epsilon$  is presented. The values of the parameters adopted for the simulations are reported in Table 4, whereas Table 5 lists the ASO average physical characteristics, taken from Ref. [10].

The left plot in Figure 7 shows the time histories of  $S$ ,  $D$ ,  $N$ , and  $B$  for both the raising and non-raising cases. In particular, solid lines are associated to MOCAT-5R, while the dashed lines to MOCAT-4B results. The right plot shows the difference between the two models,  $\Delta Q = Q_{\text{raising}} - Q_{\text{no raising}}$ . What is essential to notice is the sign of  $\Delta Q$ : if

**Table 4 Parameters employed to run the simulations.**

Parameter	Value
$h_{min}$	200 km
$h_{max}$	2000km
$n$	36
$\Delta t$	5 years
$v_{imp}$	10 km/s
$\alpha$	0.05
$\alpha_a$	0.005
$\delta$	10
$\delta_B$	10
$c_D$	2.2
$L_c$	0.1 m
$P_m$	96%
$P_d$	99.9%
$P_r$	99.95%
$t_{depl}$	10 years
$\epsilon$	5e-5 m/s <sup>2</sup>
$\bar{e}$	0.01

**Table 5 ASO Average physical characteristics.**

ASO	Mass [kg]	Diameter [m]	Area [m <sup>2</sup> ]
$S$ (active satellites)	223	1.490	1.741
$D$ (derelicts)	223	1.490	1.741
$N$ (debris)	0.640	0.180	0.020
$B$ (rocket bodies)	1421	3.070	7.419

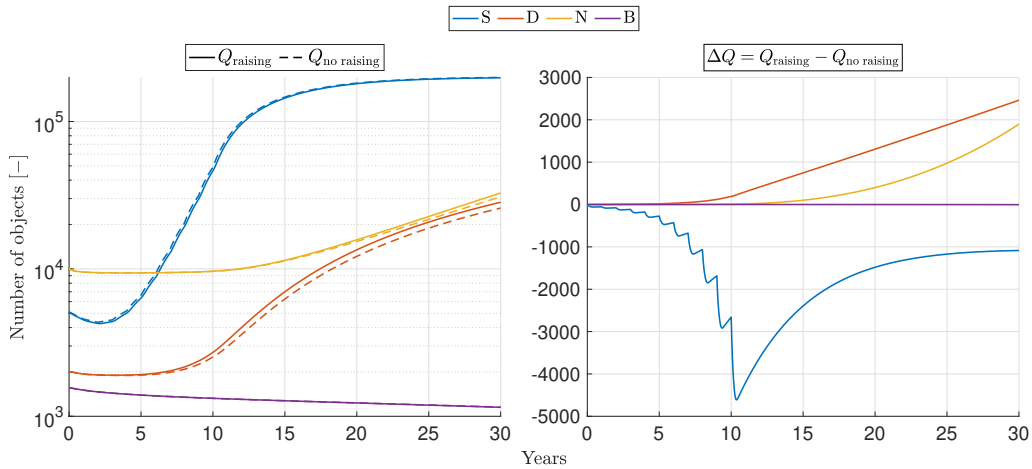


**Fig. 7 Population evolution in time and their difference for both raising (MOCAT-5R) and non-raising case (MOCAT-4B).**

positive, the raising case has more objects than the non-raising case; if negative, the other way around. The number of derelicts and debris is higher with the MOCAT-5R, and consequently, the number of satellites is lower. This is due to the higher number of satellites crossing multiple shells causing collisions and failures during orbit transfer maneuvers. No significant differences can be evinced between the rocket bodies. Concerning active satellites, the reported  $S$  for the raising case indicates the operating satellites  $S_h$ . This explains the wavy behavior of  $\Delta S$ : in MOCAT-4B the active satellites are instantaneously injected not only in their operative altitude but also in the  $S$  species. However, in MOCAT-5R, active satellites are launched as  $S_r$  species, and it requires time to transition to  $S_h$ . Finally,  $\Delta S$  increases in magnitude for the first 10 years, which corresponds to the deployment time chosen for the simulation and, thus, the exponential increment for the number of objects launched. After this first period, the number of satellites launched is kept constant and  $\Delta S$  decreases. This difference would tend to zero only if the models were propagated without interactions, obtaining the null difference of the validation case. For the same simulation, it is worth highlighting the altitude distribution of active satellites and derelicts at the final time. Figure 8 shows how  $S$ ,  $D$ , and  $N$  are spread along the shells for both the raising and non-raising cases. It is visible that both species resemble the launch rate distribution,

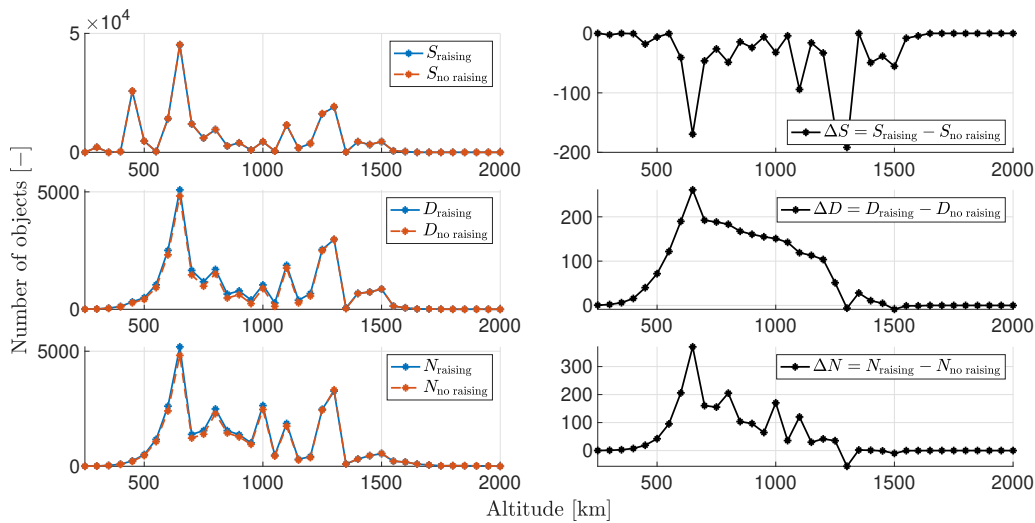


**Fig. 8 Comparison of  $S$ ,  $D$ ,  $N$ , and their difference at the final propagation time for both raising (MOCAT-5R) and non-raising case (MOCAT-4B).**

true also for  $\Delta S$ , but mirrored with respect to the x-axis. Moreover, in the  $\Delta S$  graph, it is possible to evince two negative peaks at 650 km and 1300 km, which are associated to the loss of satellites during the orbit transfer maneuvers. In fact in the non-raising case, all the satellites are assumed to be directly injected into their operative altitude. The peak at 450 km in the top-left plot is not reflected in  $\Delta S$  because that shell corresponds to one of the chosen parking orbits. On the other hand, the behavior of  $\Delta D$  is not straightforward. There are three main reasons for an active satellite becoming derelict: collision, failure in PMD, and failure during raising. The first two are directly related to the number of objects in the shells: a higher density means a higher risk of collision, and a higher number of active satellites corresponds

to a higher number of them failing PMD. These effects lead the derelicts to be a percentage of the active satellite distribution, which is what happens in the non-raising case. However, in the raising case, the failure during the orbit transfer maneuver, associated with  $P_r$  and the dynamic of  $S_r$ , strongly affects the final distribution. In the  $\Delta D$  graph, for altitudes lower than 650 km, the increasing trend is due to the combination of lower atmospheric drag and high number of satellites crossing. Instead, when the raising satellites reach the most populated shell at 650 km, the collision events become more frequent. Once this shell is passed,  $P_r$  becomes again the major source of derelicts creation. In fact, the number of derelict decreases as the altitude increases and is due to the decrease in the number of rising satellites. Finally, the negative value at 1300 km is related to the direct injection assumption for the non-raising case: since the very beginning, more satellites could fail in PMD and become derelicts. After that, another decreasing trend from 1350 km starts because of the  $P_r$  effects. Finally, the altitude distribution of debris is strongly affected by the orbital density which corresponds to the total number of objects residing in the shell. In particular,  $N$  are more easily created from collisions involving derelicts rather than active satellites, given their capability of maneuvering. Therefore, the  $N$  distribution along the shells is more similar to  $D$ . An exception is at altitude 1000 km, to which correspond the most populated region at the initial time. The  $\Delta N$  graph, as the  $\Delta D$ , shows the effects of the atmospheric drag at lower altitude. However, the differences are not as smooth as for derelicts, because the creation of debris is more related to the orbital density. The same comment done for  $D$  concerning the negative value at 1300 km can be made also for  $N$ . It is worth noticing that  $\Delta N$  is in general greater than zero, which highlight the importance of considering orbit raising in the model. To better visualize the concept, Figure 9 shows the collision events in time and altitude related to the MOCAT-5R model population. Again, most collisions involving operating satellites, derelicts, and debris are associated

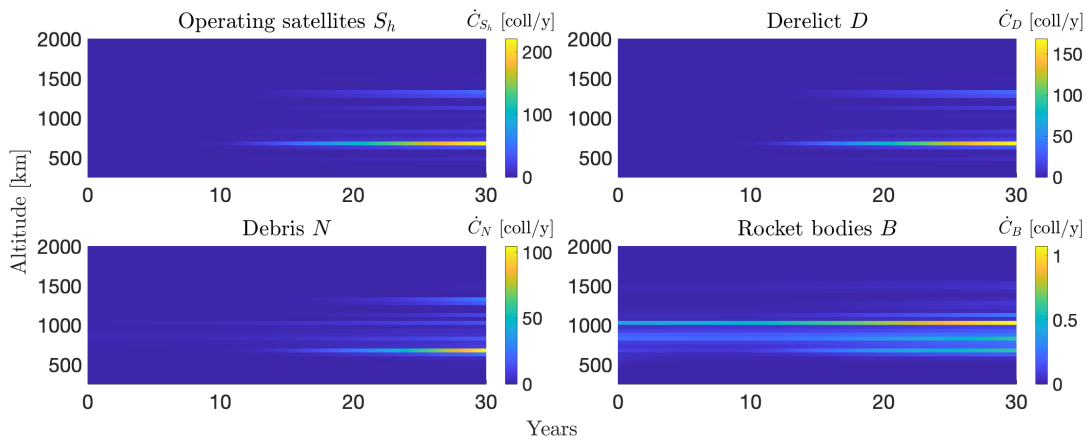


**Fig. 9 Collision events evolution in time and altitude in MOCAT-5R model.**

with the most populated shells (650 km and 1200-1300 km) because of the high number of objects present. Note that, even if the  $S_h$  become one order of magnitude bigger than  $D$  and  $N$  (see Figure. 7), the number of collision events is similar among the three species because active satellites are able to maneuver. On the contrary, as  $B$  is small, the

number of collision events involving rocket bodies is low.

Let us now consider the combined effect of raising and decay, thus the MOCAT-6RD model. The simulation is repeated with the same settings. Figure 10 shows the comparison between  $S$ ,  $D$ , and  $N$  for both raising and non-raising cases. Similar comments as for Figure 8 can be made. However, in the  $\Delta D$  plot, the effects of orbit transfer fluxes are more evident. In fact, by modeling the descent flux of satellites starting at the end of their mission lifetime, all the shells become temporarily more populated. Thus, the combination of failures (i.e.,  $P_r$  and  $P_d$ ) and the collisions cause the peak at 650 km and the monotonic decreasing trend as the altitude increases. Note that the values of  $P_r$  and  $P_d$  are constant, but  $P_d > P_r$  to model that during deorbit the probability of failure is higher, e.g., propellant depletion. Again, the positive values of  $\Delta N$  underline the importance of modelling orbit transfer maneuvers.

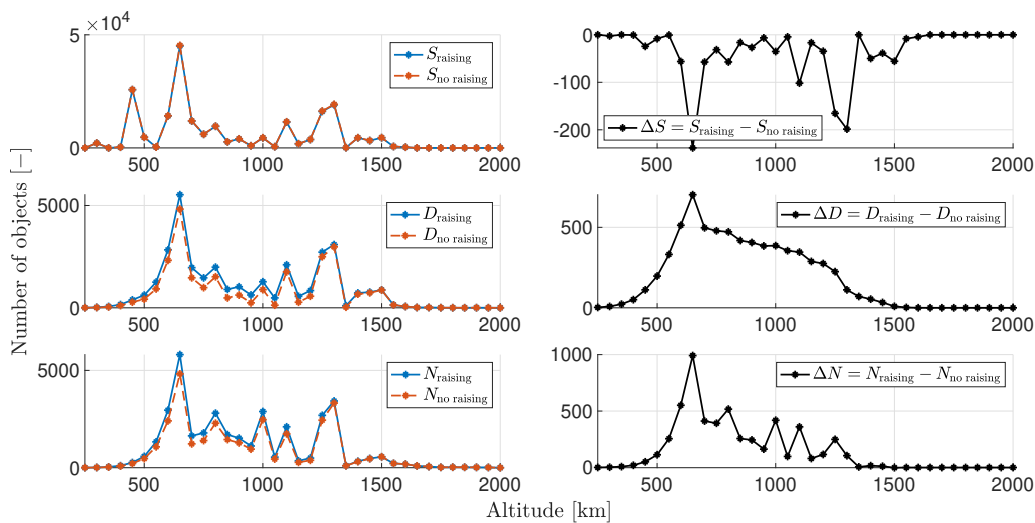


**Fig. 10 Comparison of  $S$ ,  $D$ , and  $N$ , and their difference at the final propagation time for both raising (MOCAT-6RD) and non-raising case (MOCAT-4B).**

It is also interesting to notice in Figure 11 the evolution in time and altitude of the six species. For what concerns  $S_h$ ,  $D$ , and  $N$ , the most populated shells are at 450 km, 650 km, and in between 1200-1300 km because of the high orbital density, as can be evinced from the  $S_h$  and  $D$  plots and the left plot in Figure 10. The behavior of rocket bodies is almost steady, as the shells in which more  $B$  are present correspond to a lower orbital density area around 1000 km where the atmospheric drag is not significant. Moreover, it can be noticed that at altitudes lower than 650 km, the most populated shell, the number of rocket bodies decreases due to collisions and drag effects. Finally, from  $S_r$  it is possible to clearly distinguish the second injection orbit at 450 km, while the first one is less visible because the number of satellites designated to lower altitudes is considerably lower than those launched at higher altitudes. From the same plot, it is visible the increasing trend along the first 10 years, and it can also be seen the decreasing trend as the altitude increases. Similar trends are shown in  $S_d$ : increment in the first years and convergence from higher to lower altitudes. In fact, decaying satellites must reach the first shell (200-250 km) to be considered decayed and removed.

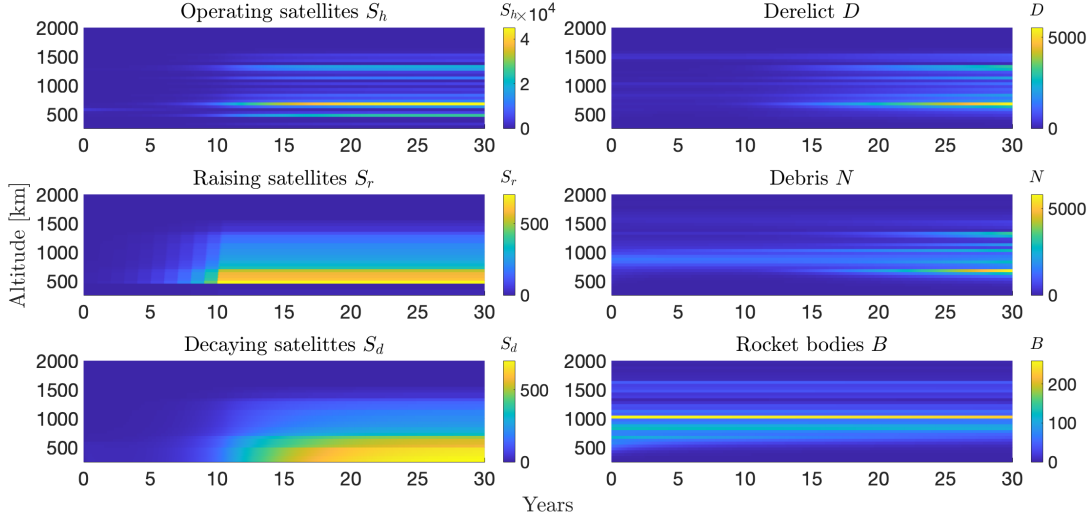


**Fig. 11 Population evolution in time and altitude in MOCAT-6RD model.**

To achieve higher accuracy in the results, a time-varying atmospheric model that considers solar activity and geomagnetic storms could be employed. This leads to a comparison between simulations using the static exponential density profile and the Jacchia-Bowman 2008 (JB2008) model. To appreciate solar cycles effects, a simulation of 60 years has been considered. Figure 12 shows, respectively on the left and on the right, the evolution in time of the MOCAT-6RD model and the percentage difference in the number of objects  $\Delta Q_{\%}$  between the static exponential and the JB2008 models defined as

$$\Delta Q_{\%} = \frac{Q_{\text{static exp.}} - Q_{\text{JB2008}}}{Q_{\text{static exp.}}} \cdot 100 \quad (36)$$

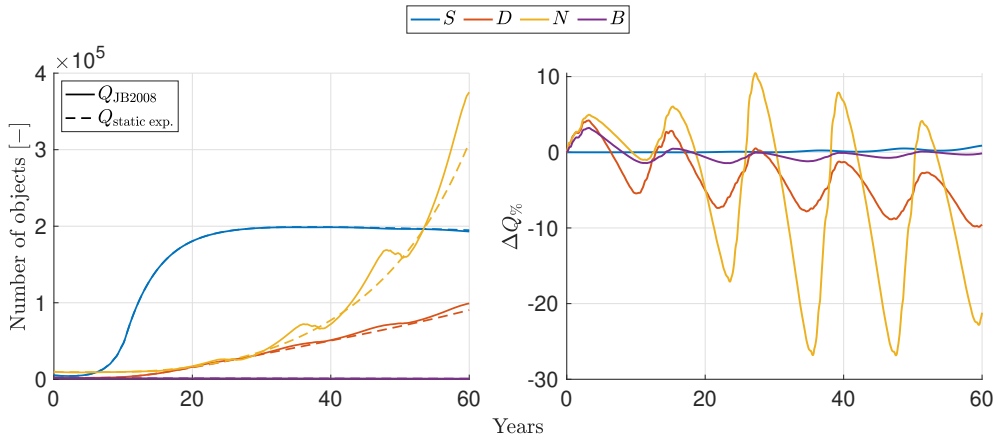


**Fig. 12 Comparison between the static exponential and the Jacchia-Bowman 2008 atmospheric model.**

Concerning the time evolution, it is clearly visible in  $D_{\text{JB2008}}$  and  $N_{\text{JB2008}}$  the dependence on the solar cycle. Rocket bodies are also affected by the time-dependent atmospheric model, but the different order of magnitude with respect to

the other species prevents it from being visible. The number of satellites, is not affected by the atmospheric model given the capability of maneuvering, however is affected by the number of objects of the other species which cause collisions. The percentage difference  $\Delta Q_{\%}$  reaches a 25% values. This magnitude highlights the importance of a time-varying atmospheric density model in order to more accurately account the impact of the solar cycle.

The JB2008-predicted densities exhibit significant variations under different levels of space weather activity. In contrast, the static exponential atmospheric model tends to overestimate drag force during low space weather activity and underestimate it during high space weather activity, as illustrated in Fig. 13. The choice between these atmospheric models depends on the simulation’s focus: for precise simulations, the JB2008 model is more appropriate, while for rapid and extensive analyses, the static exponential model provides relatively accurate results with lower computational demands. Considering the study’s nature and the need to balance computational resources, the static exponential model has been chosen for most simulations.

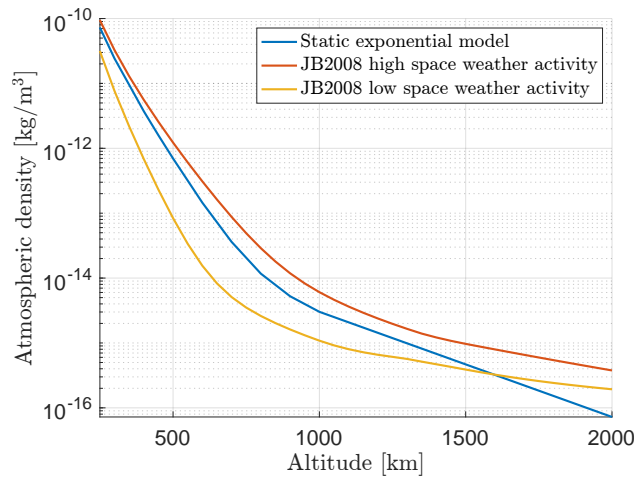
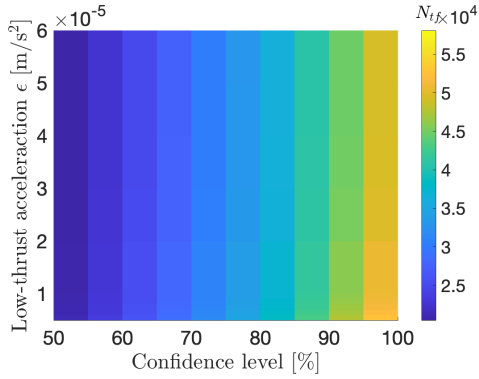


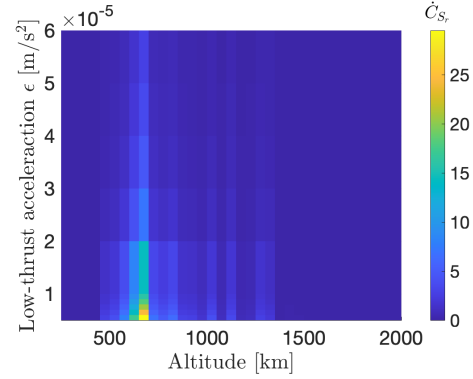
**Fig. 13 Atmospheric density over altitude variation for different models and space weather activities.**

### E. Sensitivity Analysis

Lastly, a sensitivity analysis of MOCAT-6RD with respect to the confidence level and the low-thrust acceleration magnitude is performed, while keeping fixed all the other parameters. In particular, the former spans from 50% to 100% with 5% increment, while the acceleration assumes the following values  $\epsilon = [0.5, 0.6, 0.7, 0.8, 0.9, 1, 2, 3, 4, 5, 6] \cdot 10^{-5} \text{ m/s}^2$ . The reason behind spanning the acceleration in the lower range with respect to the value used for the previous results is related to how satellites perform raising. As can be seen in Figure 5, particularly for Starlink satellites, the raising maneuvers are not direct, but the satellites perform a sort of steps, and the time passed within the shells may be higher, thus lower thrust. For simplicity the static exponential atmospheric model is used. Figure 14(a) on the left shows the final number of debris obtained at the final instant of time; Figure 14(b) on the right considers a fixed confidence level and it shows how the collision events involving raising satellites are spread among the shells. The



(a) Final number of debris obtained at the final instant of the propagation time.



(b) Raising satellites collision events in altitude with 80% confidence level.

**Fig. 14 Sensitivity analysis over confidence level and acceleration magnitude in MOCAT-6RD.**

choice of showing the number of debris at final time ( $N_{tf}$ ) is due to the fact that  $N$  is the species with the highest growth rate, as can be evinced from Figure 7, and it is not strictly related to the confidence level as much as  $S$  and  $D$  are. As expected, results show that the number of debris and collision grows for a higher confidence level, thus a higher number of satellites launched, and for a lower thrust, thus more time spent in each shell. Moreover, as the acceleration increases for a fixed confidence level, the differences in  $N_{tf}$  become less evident. The right plot, instead, considers a fixed confidence level of 80% and shows the distribution of collisions per each shell. Note that  $\dot{C}_s$  is evaluated at the final propagation time. Again, as the time necessary to raise increases, the number of collisions increases. The highest peak corresponds to the most populated shell at 650 km.

Finally, three surfaces, one per species, representing the sum of collision events over the altitudes at the final time, are shown in Figure 15. Reminding that  $S$  in the MOCAT-6RD model stands for  $S = S_h + S_r + S_d$ , the graph reports the sum of all the collisions involving active satellites without distinctions. As before, the higher the confidence level and the lower the acceleration, the higher the number of collisions for each species. The number of collisions events involving the species resembles the behaviour seen for the MOCAT-5R model visible in Figure 9, and indeed the surface related to  $D$  lays in between the other two.

## IV. Conclusions

The main novelties proposed in the paper are the introduction of the significant potential source of debris, the rocket bodies species, and the implementation of orbit transfer fluxes (raising and decay) to achieve a more realistic model. To this aim, the active satellites family is divided into three subcategories: raising, operating, and decaying satellites. Satellites can increase and lower their altitude by assuming a continuous low-thrust control. During these two phases, failures and collisions increase, yielding high orbital density shells. An attempt to study the future launch profile is proposed by analyzing historical data and the ITU's files. With all these novelties, results show the criticality of having

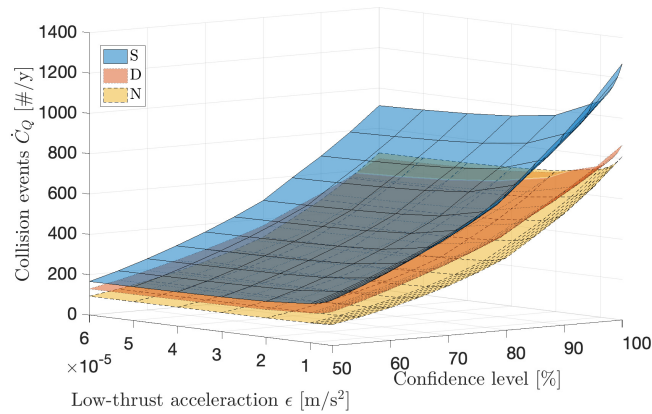


**Fig. 15** Collision events with a sensitivity analysis over confidence level and acceleration magnitude in MOCAT-6RD.

highly populated shells and the importance of reducing the failures during orbit transfer maneuvers to a minimum. Thus this tool could be used for further analysis: to compute the orbital capacity in LEO, and to quantify the risk of collision during orbit transfer, or it could also be exploited to optimize the injection orbit altitude to minimize the number of collisions and debris. In conclusion, the strength of MOCAT relies on the possibility to continuously improve the model by adding more accurate representations of the interactions between families or by performing analyses of its parameters and coefficients.

## Acknowledgments

The authors want to acknowledge the support of this work by the Defense Advanced Research Projects Agency under grant number N66001-20-1-4028.

## References

- [1] “Federal Communications Commission (FCC),” [https://licensing.fcc.gov/cgi-bin/ws.exe/prod/ib/forms/reports/swr031b.hts?q\\_set=V\\_SITE\\_ANTENNA\\_FREQ.file\\_numberC/File+Number/%3D/SATAMD2021081800105&prepare=&column=V\\_SITE\\_ANTENNA\\_FREQ.file\\_numberC/File+Number](https://licensing.fcc.gov/cgi-bin/ws.exe/prod/ib/forms/reports/swr031b.hts?q_set=V_SITE_ANTENNA_FREQ.file_numberC/File+Number/%3D/SATAMD2021081800105&prepare=&column=V_SITE_ANTENNA_FREQ.file_numberC/File+Number), 2022. Accessed: 2022-09-16.
- [2] “Federal Communications Commission (FCC),” [https://licensing.fcc.gov/cgi-bin/ws.exe/prod/ib/forms/reports/swr031b.hts?q\\_set=V\\_SITE\\_ANTENNA\\_FREQ.file\\_numberC/File+Number/%3D/SATLOA2021110400145&prepare=&column=V\\_SITE\\_ANTENNA\\_FREQ.file\\_numberC/File+Number](https://licensing.fcc.gov/cgi-bin/ws.exe/prod/ib/forms/reports/swr031b.hts?q_set=V_SITE_ANTENNA_FREQ.file_numberC/File+Number/%3D/SATLOA2021110400145&prepare=&column=V_SITE_ANTENNA_FREQ.file_numberC/File+Number), 2022. Accessed: 2022-09-16.
- [3] “Federal Communications Commission (FCC),” [https://licensing.fcc.gov/cgi-bin/ws.exe/prod/ib/forms/reports/swr031b.hts?q\\_set=V\\_SITE\\_ANTENNA\\_FREQ.file\\_numberC/File+Number/%3D/SATLOA2021110400140&prepare=&column=V\\_SITE\\_ANTENNA\\_FREQ.file\\_numberC/File+Number](https://licensing.fcc.gov/cgi-bin/ws.exe/prod/ib/forms/reports/swr031b.hts?q_set=V_SITE_ANTENNA_FREQ.file_numberC/File+Number/%3D/SATLOA2021110400140&prepare=&column=V_SITE_ANTENNA_FREQ.file_numberC/File+Number), 2022. Accessed: 2022-09-16.

- [4] Liou, J.-C., Hall, D., Krisko, P., and Opiela, J., “LEGEND—A three-dimensional LEO-to-GEO debris evolutionary model,” *Advances in Space Research*, Vol. 34, No. 5, 2004, pp. 981–986. <https://doi.org/10.1016/j.asr.2003.02.027>.
- [5] Lewis, H. G., Swinerd, G., Williams, N., and Gittins, G., “DAMAGE: a dedicated GEO debris model framework,” *Space Debris*, Vol. 473, 2001, pp. 373–378.
- [6] Walker, R., Martin, C., Stokes, P., Wilkinson, J., and Klinkrad, H., “Analysis of the effectiveness of space debris mitigation measures using the DELTA model,” *Advances in Space Research*, Vol. 28, No. 9, 2001, pp. 1437–1445. [https://doi.org/10.1016/S0273-1177\(01\)00445-8](https://doi.org/10.1016/S0273-1177(01)00445-8).
- [7] Talent, D. L., “Analytic model for orbital debris environmental management,” *Journal of spacecraft and rockets*, Vol. 29, No. 4, 1992, pp. 508–513. <https://doi.org/10.2514/3.25493>.
- [8] Somma, G. L., Colombo, C., and Lewis, H., “A statistical LEO model to investigate adaptable debris control strategies,” *7th European Conference on Space Debris, ESA/ESOC*, ESA, 2017, pp. 1–12.
- [9] Somma, G. L., “Adaptive remediation of the space debris environment using feedback control,” Ph.D. thesis, University of Southampton, 2019. URL <https://eprints.soton.ac.uk/403265/>.
- [10] Trozzi, V., Colombo, C., and Trisolini, M., “Analysis of possible definitions of the space environment capacity to pursue long-term sustainability of space activities,” *72nd International Astronautical Congress (IAC 2021)*, 2021, pp. 1–14.
- [11] Krag, H., Lemmens, S., and Letizia, F., “Space traffic management through the control of the space environment’s capacity,” *1st IAA Conference on Space Situational Awareness (ICSSA)*, Orlando, FL, US, 2017.
- [12] Rossi, A., Valsecchi, G., and Alessi, E., “The criticality of spacecraft index,” *Advances in Space Research*, Vol. 56, No. 3, 2015, pp. 449–460. <https://doi.org/10.1016/j.asr.2015.02.027>.
- [13] A. D’Ambrosio, R. L., M. Lifson, “The Capacity of Low Earth Orbit Computed using Source-sink Modeling,” *arXiv*, 2022. <https://doi.org/10.48550/ARXIV.2206.05345>, accessed: 2022-09-6.
- [14] Lifson, M., D’Ambrosio, A., Arnas, D., and Linares, R., “How Many Satellites Can We Fit in Low Earth Orbit?: Capacity integrating Risk-based and Intrinsic Methods,” *2022 AAS/AIAA Astrodynamics Specialist Conference, Charlotte, North Carolina, August 7-11, 2022*.
- [15] D’Ambrosio, A., Servadio, S., Siew, P. M., Jang, D., Lifson, M., and Linares, R., “Analysis of the LEO orbital capacity via probabilistic evolutionary model,” *2022 AAS/AIAA Astrodynamics Specialist Conference, Charlotte, North Carolina, August 7-11, 2022*.
- [16] D’Ambrosio, A., Servadio, S., Siew, P. M., and Linares, R., “A novel source-sink model for space environment evolution with orbit capacity assessment,” *Journal of Spacecraft and Rockets*, 2023. <https://doi.org/10.2514/1.A35579>.
- [17] Jang, D., D’Ambrosio, A., Lifson, M., Pasiecznik, C., and Linares, R., “Stability of the LEO Environment as a Dynamical System,” *Advanced Maui Optical and Space Surveillance Technologies (AMOS) Conference*, 2022.

- [18] Pasiecznik, C., D'Ambrosio, A., Jang, D., and Linares, R., "A Dynamical System Analysis of the Effectes of the Launch Rate Distribution on the Stability of a Source-Sink Orbital Debris Model," *International Astronautical Congress*, International Astronautical Federation, IAF, Paris, France, 2022.
- [19] D'Ambrosio, A., Lifson, M., Jang, D., Pasiecznik, C., and Linares, R., "Projected Orbital Demand and LEO Environmental Capacity," *Advanced Maui Optical and Space Surveillance Technologies (AMOS) Conference*, 2022.
- [20] Krisko, P., "Proper implementation of the 1998 NASA breakup model," *Orbital Debris Quarterly News*, Vol. 15, No. 4, 2011, pp. 1–10. URL <https://orbitaldebris.jsc.nasa.gov/quarterly-news/pdfs/odqnv15i4.pdf>, accessed: 2022-09-14.
- [21] Lemmens, S., and Letizia, F., "ESA's annual space environment report," Tech. rep., Technical Report GEN-DB-LOG-00288-OPS-SD, ESA Space Debris Office, 2021.
- [22] Pardini, C., and Anselmo, L., "Review of past on-orbit collisions among cataloged objects and examination of the catastrophic fragmentation concept," *Acta Astronautica*, Vol. 100, 2014, pp. 30–39.
- [23] Vallado, D. A., *Fundamentals of Astrodynamics and Applications*, Vol. 4th edn., Edited by T. S. T. Library. Hawthorne, CA: Microcosm Press and Springer, 2013.
- [24] Bowman, B., Tobiska, W. K., Marcos, F., Huang, C., Lin, C., and Burke, W., "A new empirical thermospheric density model JB2008 using new solar and geomagnetic indices," *AIAA/AAS astrodynamics specialist conference and exhibit*, 2008, p. 6438. <https://doi.org/10.2514/6.2008-6438>.
- [25] Di Carlo, M., and Vasile, M., "Analytical solutions for low-thrust orbit transfers," *Celestial Mechanics and Dynamical Astronomy*, Vol. 133, No. 7, 2021, pp. 1–38. <https://doi.org/10.1007/s10569-021-10033-9>.
- [26] "Space-Track," <https://www.space-track.org>, 2022. Accessed: 2022-10-05.
- [27] "DISCOSWeb," <https://discosweb.esoc.esa.int>, 2022. Accessed: 2022-10-05.
- [28] "CelesTrak," <https://celestrak.org>, 2022. Accessed: 2022-10-05.